Influence of tungsten-doping on the acid sites and redox properties of COS+CS_2 sulfating $Ce_{0.5}Fe_{0.5}O_x$-S catalyst for NH_3-SCR reaction: Regulating of promoted Fe-W interaction on the formation of sulfate species

Mengyao Wang[1*], Jingsong Zhou[1*], Yanping Du[2*], Yafei Zhu[1], Zhou Liu[3], Fei Zhou[3], Zhenchang Sun[1], Wei Lu[1], Zhibo Xiong[1**]

(1. School of Energy and Power Engineering, University of Shanghai for Science & Technology, Shanghai, 200093, China

2. School of Engineering, Lancaster University, Lancaster, LA1 4YW, UK

3. Jiangsu Guoxin Research Institute Co, Ltd., Nanjing, 210000, Jiangsu, China)

Abstract: Herein, as typical solid acidic oxides, Tungsten was doped into the $Ce_{0.5}Fe_{0.5}O_x$-S catalyst to modulate its gas-phase sulfation by organic COS+CS_2, which enhanced the NH_3-SCR activity at low-medium temperatures, with an optimal doping molar ratio of W/(Ce+Fe) is 0.3. The characterization indicated that tungsten doping inhibited the adsorption and conversion of COS+CS_2 over the catalyst due to the enhanced interaction between iron and tungsten species. This effect diminished the diffraction peaks of iron sulfate and α-Fe_2O_3 at a W/(Ce+Fe) ratio of 0.5. The promoted Fe–W interaction also increased oxygen vacancies and enriched the pore structure. However, crystalline WO_3 formed at high doping levels shielded the Raman signals of cubic fluorite CeO_2 and surface oxygen vacancies, partially blocking pores and reducing the BET surface area. Interestingly, this promoted interaction increased the surface concentrations of both Ce^{3+} and Fe^{3+}, and the $Ce_{0.5}Fe_{0.5}W_{0.3}O_x$-S catalyst even presented a larger surface concentration of Fe species than the $Ce_{0.5}Fe_{0.5}O_x$-S catalyst, although tungsten doping decreased the concentration of Ce species significantly. Furthermore, this promoted interaction reduced the amount of sulfates formed in the catalyst by restraining the gas-phase sulfation of Ce/Fe species, thereby regulating the total acid sites and weak acid sites/total acid sites proportion of $Ce_{0.5}Fe_{0.5}O_x$-S catalyst due to the different roles of the solid acidity of tungsten oxides and S^{6+} species in the formation of acid sites in W-doped $Ce_{0.5}Fe_{0.5}O_x$-S catalyst. It was found that both high levels of sulfate ions and tung -ten doping contributed to increasing the total acid sites of the catalyst.

* The Co-first authors: Mengyao Wang, Jingsong Zhou and Yanping Du.

* * Corresponding author: Zhibo Xiong, Tel.: +86 21 55272320, Email addresses: xzb412@usst.edu.cn (Z.Xiong)

Keywords: NO_x reduction, Cerium-iron mixed oxide catalyst, Tungsten-doping, Sulfating, Regulation

1. Introduction

Due to its high efficiency, ammonia selective catalytic reduction (NH_3-SCR) is one of the most widely used technologies to control the emission of nitrogen oxides (NO, NO_2, etc.) from the stationary and mobile sources [1,2]. However, the commercial V_2O_5-WO_3(MoO_3)/TiO_2 catalyst still presents the disadvantages of a narrow reaction temperature window (300-400 °C), V-biological toxicity and low N_2 selectivity at high temperature [3,4]. The transition metal iron has attracted much attention owing to the non-toxicity and economy, which have been expected to be developed into the environmentally friendly catalysts for NH_3-SCR reaction.

Based on the electron transfer between Ce^{3+}/Ce^{4+}, CeO_2 presents good redox properties by strongly storing-releasing oxygen, and its doping has been found to improve the NH_3-SCR activity of iron oxide catalyst owing to the promoted interaction of $Ce^{4+}+Fe^{2+}\rightarrow Ce^{3+}+Fe^{3+}$. However, the shortcomings of poor low-temperature activity and high-temperature NH_3-peroxidation still needs to be overcome before the practical applications of iron-cerium mixed oxide catalysts [5-7]. The enhancement of surface acid sites contributed to improving the low-temperature NH_3-SCR activity of this mixed oxide catalyst and broadening its active reaction temperature window [8]. At present, the treatment of sulfation, including H_2SO_4 or/and metal sulfates impregnation and sulfur-containing gas-phase pre-sulfurization, has been confirmed as an effective means to improve the surface acidity and de-nitrification performance of cerium-based catalysts by introducing S^{6+} species [9]. Kang et al. found that a simple impregnation pretreatment of H_2SO_4 solution significantly enhanced the medium and high temperature (350-500 °C) de-nitration activity of FeZrCeTiO_x/TNT catalyst, mainly attributing to the enhanced Brönsted acid sites of catalyst, which promoted the adsorption and activation of NH_3 molecules and simultaneously inhibited the excessive adsorption of NO_x [10]. Song et al. pointed out that the gas-phase sulfation of SO_2 resulted in the formation of sulfates on the surface of Fe-Ce catalyst, which promoted the transformation of Lewis acid sites to Brönsted acid sites on the catalyst surface and accelerated the conversion of low-activity nitric acid to high-activity nitrate during the NH_3-SCR reaction. This

played an important role in broadening the catalytic activity window [11]. Our previous researches demonstrated that organic COS or/and CS_2 exhibited stronger promotional effect on the NH_3-SCR activity of CeO_2 catalyst than inorganic SO_2, especially CS_2 [12]. Compared to SO_2, the gas-phase sulfation of COS or/and CS_2 resulted in more Ce^{3+}, defect sites and Brönsted acid sites formed on the catalyst surface. And the introduction of H_2O or/and O_2 during the gas-phase sulfation further improved the promotional effect of COS+CS_2 treatment on the NH_3-SCR activity of CeO_2 catalyst [13-15].

As typical solid acidic oxides, tungsten or/and molybdenum oxides also have been introduced to increase the NH_3-SCR activity and anti-SO_2 poisoning of Cerium-based catalysts by optimizing the acid sites and acting as sulfur capture sites [16]. Cheng et al. found that the introduction of 15 wt.% WO_3 resulted in the formation of tungsten oxide microcrystalline on the surface of $MnCeO_x$ catalyst, which not only increased the surface concentrations of Ce^{3+} and Mn^{4+}, but also enhanced the acid sites of catalysts, and the modified catalyst presented an excellent NH_3-SCR activity and anti-SO_2/H_2O poisoning [17]. Nam et al. pointed out that the thermal stability of Brönsted acid sites of Ce-based catalyst was improved by doping tungsten additives, which promoted both NH_3 adsorption and NO conversion to NO_2 on the catalyst surface, thereby increased the low-temperature NH_3-SCR activity of catalyst [18]. Therefore, similar to the optimizing acid sites of S^{6+} species via sulfation, the introduction of tungsten oxide also helped to increase the NH_3-SCR activity of cerium-based catalyst by improving the acid sites, but they presented different effects on the other physico-chemical properties of catalysts. Arfaoui et al. found that the modification of sulfuric acid (SO_4^{2-}) contributed to improving the dispersion of active components via the interaction of Ce and SO_4^{2-} species, which increased the high-temperature catalytic performance of CeO_2-TiO_2 catalyst by inducing new strong acid sites. While tungsten doping generated more oxygen vacancies and new redox sites on the catalyst surface, thereby promoted the low-temperature NH_3-SCR activity of CeO_2-TiO_2 catalyst although it had little effect on the surface acidity of catalyst [19]. Actually, as a auxiliary agent, tungsten oxide was also doped to improve the anti-O_2 poisoning of Al-base catalyst for the catalytic hydrolysis of COS or/and CS_2 by depressing the sulfation of active components (Al etc.). Therefore, tungsten doping contributes to regulating the conversion of COS or/and CS_2 on the surface of cerium-based catalyst and influences their interaction with active components, thereby may affect the physical-chemical

properties and activity of the corresponding sulfated catalyst for NH_3-SCR reaction.

In this study, tungsten doping was employed to regulate the conversion of COS+CS_2 on the surface of the $Ce_{0.5}Fe_{0.5}O_x$ catalyst in the presence of O_2+H_2O. The doping molar ratio of tungsten was found to significantly influence the amount of SO_4^{2-} species formed on the surface of sulfated $Ce_{0.5}Fe_{0.5}O_x$-S catalyst, with $Ce_{0.5}Fe_{0.5}W_{0.3}O_x$-S presenting the highest NH_3-SCR activity. Characterization results revealed that tungsten doping suppressed the formation and adsorption of SO_4^{2-} species through a promoted interaction between Fe and W, which not only modulated the acid sites of the catalyst but also enriched its oxygen vacancy.

2. Experimental

2.1. Catalyst preparation

A series of $Ce_{0.5}Fe_{0.5}W_aO_x$-S (a = 0, 0.1, 0.3, 0.5) catalysts were prepared by one-pot hydrothermal method, where a represents the molar ratio of W/(Ce+Fe+W), and the molar ratio of cerium and iron is kept at 1:1. Cerium nitrate, ferric nitrate, ammonium meta-tungstate, ammonium bicarbonate and hydrogen peroxide were used as metal sources, precipitant and oxidant, respectively. $Ce(NO_3)_3{\cdot}6H_2O$ and $Fe(NO_3)_3{\cdot}9H_2O$ were dissolved in 15 mL de-ionized water and stirred for 2 h, and then 0.02 mol ammonium bicarbonate (NH_4HCO_3) was dissolved in 15 mL de-ionized water and stirred for 0.5 h. The mixed solution was slowly added to the solution of NH_4HCO_3 for reverse precipitation and stirred for 0.5 h. A certain amount of ammonium meta-tungstate ($H_{28}N_6O_{41}W_{12}$) was dissolved in 9 mL H_2O_2 (10 mol/L) solution and stirred for 0.5 h. And then, the mixed solution of H_2O_2 and ammonium meta-tungstate was added to the mixed turbid solution and stirred for 3h. Subsequently, the solution was transferred to a 100 mL Teflon-lined high-pressure reactor and heated at 200 ºC for 6 h. After the hydrothermal process is completed, the reaction kettle is cooled with water, and the obtained precipitate is alternately washed and filtered several times with de-ionized water and anhydrous ethanol. Finally, the precipitate was dried at 80 ºC for 12 h and calcined at 400 ºC for 5 h in air atmosphere. The as-prepared catalyst was sieved to a particle size of 40-60 mesh, and then 0.45 g catalyst was placed in a quartz tube and sealed with quartz cotton. The sulfated catalyst was named $Ce_{0.5}Fe_{0.5}W_aO_x$-S after the gas-phase sulfation of COS+CS_2 at 50 ºC for 3 h in a tube furnace. The composition of sulfide gas is as follows: the total concentration of S element is 200 ppm,

COS:CS_2=7: 3, 5 vol. % O_2, 0.33 vol.% H_2O, N_2 is the equilibrium gas, and the total gas flow rate is 500 mL/min.

2.2. Catalytic activity test and characterization

The NH_3-SCR activity of catalysts was evaluated in a fixed-bed quartz tube micro-reactor using 0.45 g of catalyst (40~60 mesh) positioned in the center and sealed with quartz cotton. The concentrations of O_2 and NO_x at inlet and outlet were continuously monitored by a T-350 flue gas analyzer (Testo, Germany), and the NO_x conversion rate (η) was calculated according to the following formula: $\eta = (1-[NO_x]_{out}/[NO_x]_{in})\times 100\%$, where $[NO_x]_{in}$ and $[NO_x]_{out}$ represent the inlet and outlet concentrations of NO_x (NO and NO_2), respectively. Furthermore, X-ray diffraction (XRD), Raman spectroscopy (Raman), N_2 adsorption-desorption, Scanning electron microscopy (SEM), High-resolution transmission electron microscopy (HR-TEM), X-ray photoelectron spectroscopy (XPS), Thermo-gravimetric (TG), Temperature programmed reduction of H_2 (H_2-TPR) and Temperature programmed desorption of NH_3 (NH_3-TPD) were employed to study the effect of W-doping on the physicochemical properties of $Ce_{0.5}Fe_{0.5}O_x$-S catalyst. Detailed characterization procedures are provided in the Supporting Information (SI).

3. Results and discussion

3.1 Catalytic performance and XRD patterns

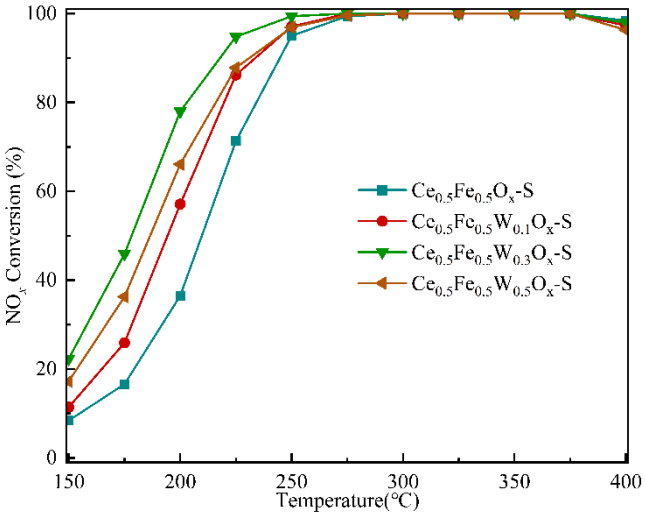

Fig.1. Influence of tungsten doping on the NH_3-SCR activity of $Ce_{0.5}Fe_{0.5}O_x$-S catalyst. (Reaction conditions: $[NH_3]$ =[NO]=600 ppm, 5.0 vol.% O_2 balanced with N_2 and GHSV=200,000 mL/(g·h)).

Fig.1 illustrates the effect of tungsten doping on the NH_3-SCR activity of $Ce_{0.5}Fe_{0.5}O_x$-S catalyst, and it is found that tungsten doping significantly increases the reduction of NO_x over

$Ce_{0.5}Fe_{0.5}O_x$-S catalyst below 250 °C, with the optimal W/(Ce+Fe) molar ratio of 0.3. Compared to $Ce_{0.5}Fe_{0.5}W_{0.1}O_x$-S and $Ce_{0.5}Fe_{0.5}W_{0.5}O_x$-S catalysts, $Ce_{0.5}Fe_{0.5}W_{0.3}O_x$-S exhibits the widest operating temperature window for the NH_3-SCR reaction, achieving a de-nitration efficiency close to 80 % at 200 °C under a GHSV of 200,000 mL/(g·h), which is higher than the reported Ce-based catalyst summarized in the Table S1 in Supporting Information. According to the XRD patterns of catalysts in Fig.2, the $Ce_{0.5}Fe_{0.5}O_x$-S catalyst displays diffraction peaks corresponding to α-Fe_2O_3 (PDF#33-0664), cubic fluorite CeO_2 (PDF#34-0394), and $Fe_6S_8O_{33}$ (PDF#21-0921), and the detection of $Fe_6S_8O_{33}$ provides unambiguous evidence for the successful adsorption and subsequent conversion of the COS+CS_2 during the sulfation process[20]. Upon tungsten doping, the intensities of α-Fe_2O_3 and CeO_2 peaks are significantly reduced, and the $Fe_6S_8O_{33}$ peaks disappear, indicating that tungsten suppresses COS + CS_2 adsorption and conversion. Increasing the W/(Ce+Fe) molar ratio from 0.1 to 0.3 further enhances this effect, with α-Fe_2O_3 peaks no longer detectable for $Ce_{0.5}Fe_{0.5}W_{0.3}O_x$-S, suggesting strong Fe-W interactions. In addition, only a wide diffraction peak located at 15-35 ° is detected for $Ce_{0.5}Fe_{0.5}W_{0.5}O_x$-S catalyst, and its main diffraction peak towards the left compared with those cubic fluorite structure CeO_2 of the other catalysts. This shift implies that excessive doping amount of tungsten actually affect the interaction of cerium and iron species, which makes the XRD patterns of α-Fe_2O_3 to disappear and even leads the diffraction peaks of cubic fluorite structure CeO_2 shifting to left due to the sedimentation and aggregation of WO_x nanoparticles [21]. It should be mentioned that no diffraction peaks attributed to WO_x are detected in $Ce_{0.5}Fe_{0.5}W_{0.1}O_x$-S and $Ce_{0.5}Fe_{0.5}W_{0.5}O_x$-S catalysts, indicating that it may present in the form of an amorphous phase or/and the undetectable micro-crystals by X-ray diffractometer [22].

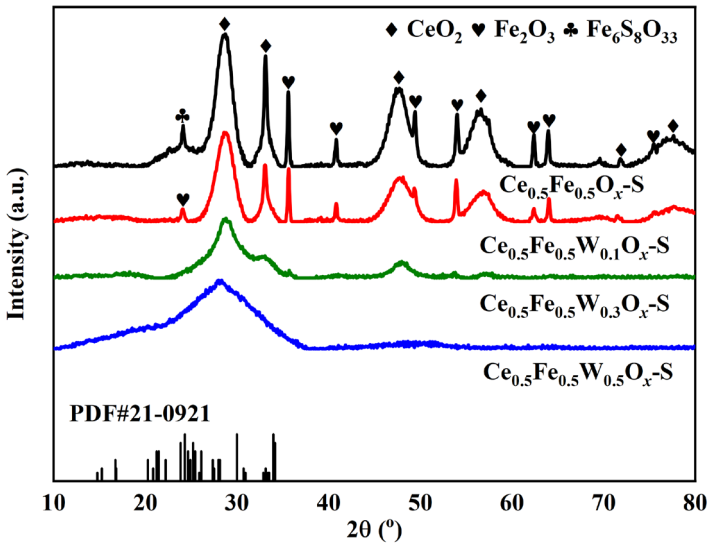

Fig. 2. Influence of tungsten doping on the XRD patterns of $Ce_{0.5}Fe_{0.5}O_x$-S catalyst

3.2 Raman and N_2 adsorption-desorption

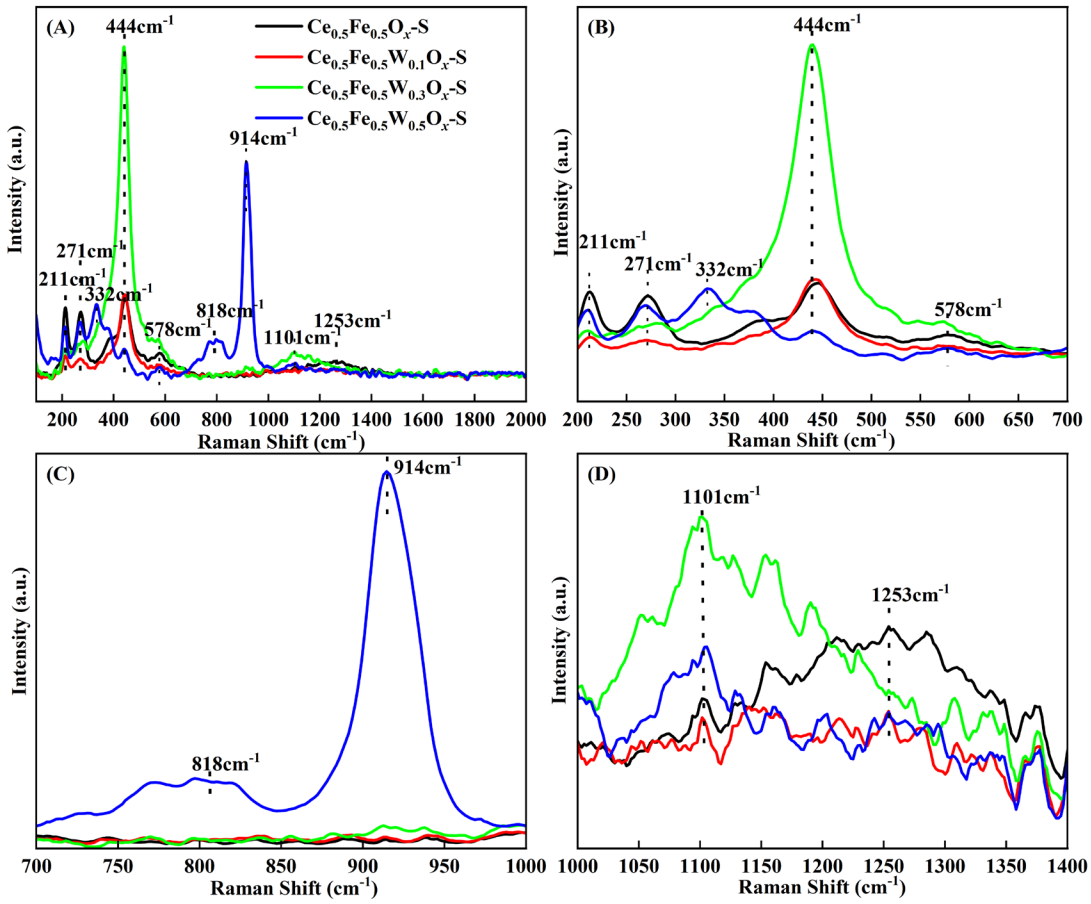

Fig. 3. Influence of tungsten doping on Raman spectra of $Ce_{0.5}Fe_{0.5}O_x$-S catalyst: Overall view (A) and Local enlarged views (B-D).

The structural features and defects of the samples were further probed by Raman

spectroscopy, as shown in Fig. 3. The Raman spectra of the $Ce_{0.5}Fe_{0.5}O_x$-S catalyst reflect the characteristic peaks of its two constituent phases, the α-Fe_2O_3 phase located at approximately 211 and 271 cm^{-1} [23, 24], and the cubic fluorite CeO_2 phase with F_{2g} vibration, defect (D) mode and second-order longitudinal optical (2LO) mode located at 444, 578 and 1253 cm^{-1}, respectively [25]. These indicates the presence of α-Fe_2O_3 and cubic fluorite structure CeO_2 in $Ce_{0.5}Fe_{0.5}O_x$-S catalyst. However, $Ce_{0.5}Fe_{0.5}W_{0.1}O_x$-S exhibits weaker Raman spectra peaks attributing to α-Fe_2O_3 than $Ce_{0.5}Fe_{0.5}O_x$-S, indicating tungsten doping with the molar ratio of W/(Ce+Fe) being 0.1 decreases the crystallization strength of α-Fe_2O_3 and there exists a good interaction of Fe and doped W, which are in-accordance with the XRD patterns in Fig .2. Furthermore, this doping also reduces the strength of Raman spectra peaks ascribing to the defect-induced (D) mode and the second-order longitudinal optical (2LO) mode of CeO_2. Interestingly, the enhancement of tungsten doping molar ratio to 0.3 significantly increases the intensity of Raman peaks attributing to CeO_2 of catalyst, especially its F_{2g} vibration mode, indicating the stronger interaction of iron and doped tungsten species and more oxygen vacancies formed on the surface of $Ce_{0.5}Fe_{0.5}W_{0.3}O_x$-S catalyst [26]. However, some Raman peaks appear in the range of 700-1000 cm^{-1} for $Ce_{0.5}Fe_{0.5}W_{0.5}O_x$-S catalyst, which can be attributed to tungsten oxide species, demonstrating the further enhancement of W/(Ce+Fe) molar ratio to 0.5 results in the formation of WO_3 crystal on the surface of catalyst, and the Raman peaks of CeO_2 or/and oxygen vacancies were almost shielded [27]. Therefore, the tungsten doping molar ratio plays a key role in regulating the interaction between cerium and iron species in the $Ce_{0.5}Fe_{0.5}O_x$-S catalyst, leading to variations in surface oxygen vacancies, which are considered crucial for enhancing the NH_3-SCR catalytic activity.

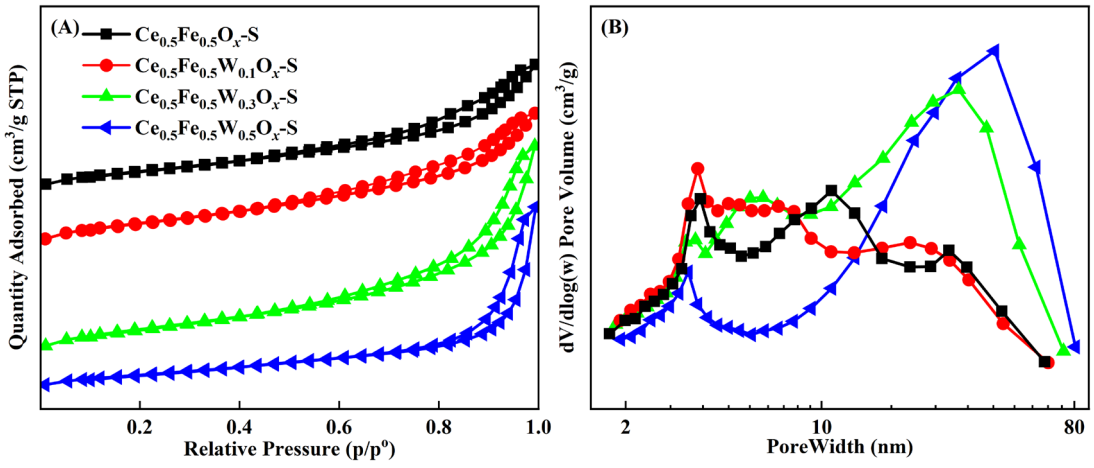

Fig. 4. Influence of tungsten doping on pore structure of $Ce_{0.5}Fe_{0.5}O_x$-S catalyst: N_2 adsorption-desorption isotherms (A) and Pore size distributions (B).

Fig. 4 shows the effect of tungsten doping on the N_2 adsorption-desorption behavior and pore size distribution of the $Ce_{0.5}Fe_{0.5}O_x$-S catalyst. From Fig. 4(A), the N_2 adsorption-desorption isotherms of all catalysts assign to the type IV with a distinct H3-type hysteresis loop according to the IUPAC classification, which is characteristic of mesoporous materials formed by the aggregation of nanoparticles [28]. However, the enhancement of tungsten doping molar ratio leads the closure point of N_2 adsorption-desorption isotherm of $Ce_{0.5}Fe_{0.5}O_x$-S catalyst first shift to low pressure, and then move to high pressure. And $Ce_{0.5}Fe_{0.5}W_{0.1}O_x$-S and $Ce_{0.5}Fe_{0.5}W_{0.3}O_x$-S have smaller pressure closure points and more mesoporous structures [22]. The pore size distributions in Fig. 4(B) demonstrate that $Ce_{0.5}Fe_{0.5}W_{0.1}O_x$-S exhibits larger mesoporous locating at 2-8 nm than $Ce_{0.5}Fe_{0.5}O_x$-S catalyst, although they both present wider pore size distribution. However, further increasing the tungsten doping molar ratio may cause blockage of mesopores around 2 nm, while enlarging the mesoporous structures near 80 nm. Notably, $Ce_{0.5}Fe_{0.5}W_{0.1}O_x$-S exhibits a well-developed gradient pore distribution, which is considered an important factor contributing to its NH_3-SCR activity [22]. Furthermore, according to the calculated results in Table 1, the BET surface area and pore volume of $Ce_{0.5}Fe_{0.5}O_x$-S first increases and then decreases with the enhancement of tungsten doping molar ratio from 0.1 to 0.5, and $Ce_{0.5}Fe_{0.5}W_{0.1}O_x$-S indeed has the largest BET surface area and pore volume among these catalysts. Therefore, the interaction between iron and tungsten species contributes to enriching and regulating the pore structure of $Ce_{0.5}Fe_{0.5}O_x$-S. However, the formation of WO_3 crystals at a doping molar ratio of W/(Ce+Fe) = 0.5 leads to partial pore blockage and consequently reduces the BET surface area of the catalyst. It is generally accepted that a larger specific surface area facilitates the exposure of more active sites for the NH_3-SCR reaction, thereby enhancing the adsorption and activation of NH_3 and/or NO_x on the catalyst surface [29].

Table 1. BET specific surface areas, pore volumes and average pore sizes of W doping $Ce_{0.5}Fe_{0.5}O_x$-S catalysts.

Samples	S_{BET} (m^2/g)	Pore volume(cm^3/g)	Average pore size(nm)
$Ce_{0.5}Fe_{0.5}O_x$-S	129.12	0.245	7.07
$Ce_{0.5}Fe_{0.5}W_{0.1}O_x$-S	139.57	0.250	6.74

$Ce_{0.5}Fe_{0.5}W_{0.3}O_x$-S	145.64	0.377	9.48
$Ce_{0.5}Fe_{0.5}W_{0.5}O_x$-S	100.13	0.330	13.97

3.3 SEM and HR-TEM

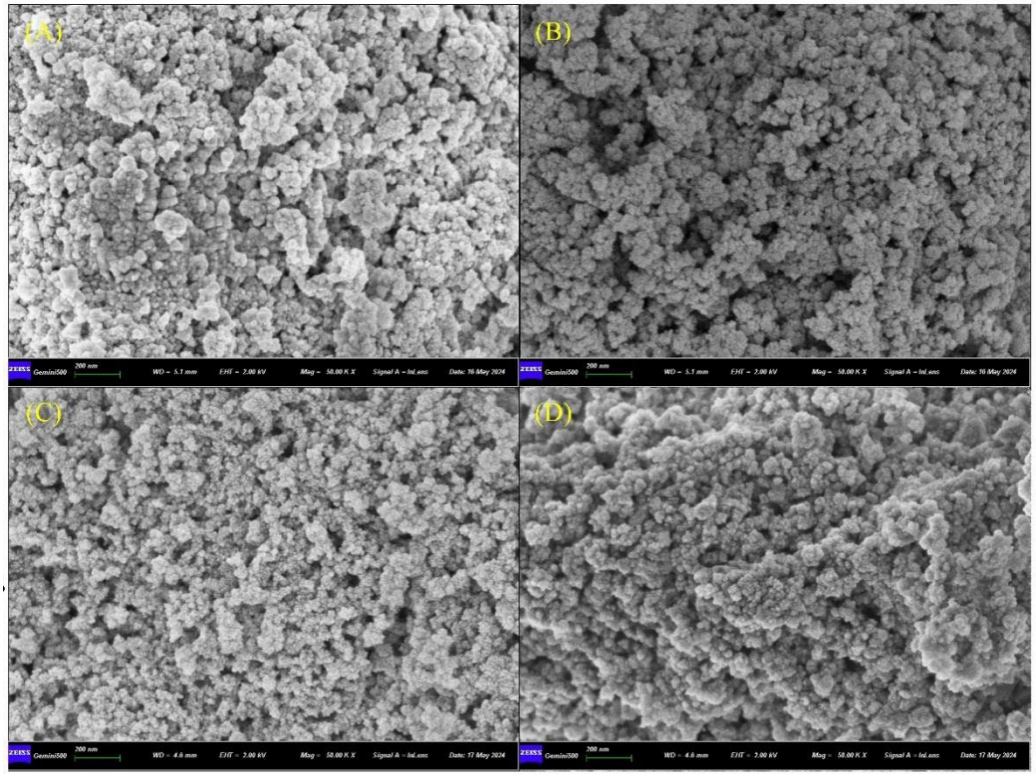

Fig.5. Influence of tungsten doping on SEM images of $Ce_{0.5}Fe_{0.5}O_x$-S catalyst: (A) $Ce_{0.5}Fe_{0.5}O_x$-S, (B) $Ce_{0.5}Fe_{0.5}W_{0.1}O_x$-S, (C) $Ce_{0.5}Fe_{0.5}W_{0.3}O_x$-S and (D) $Ce_{0.5}Fe_{0.5}W_{0.5}O_x$-S catalysts.

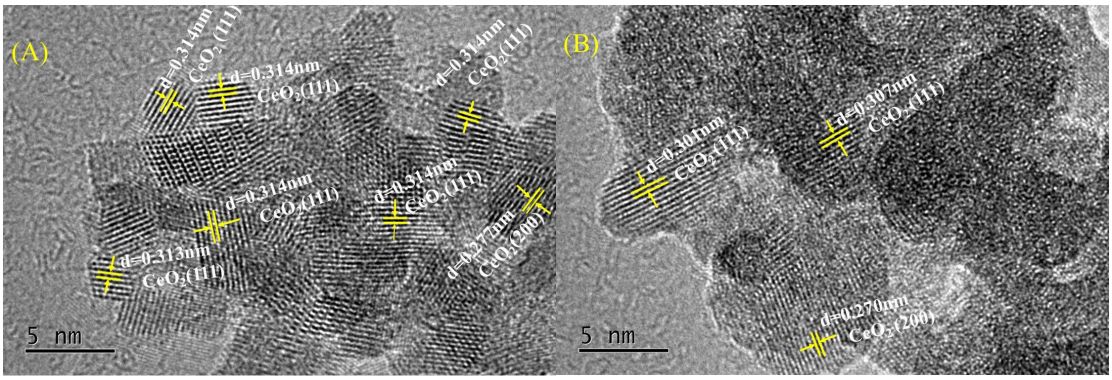

Fig. 6. HR-TEM images of $Ce_{0.5}Fe_{0.5}O_x$-S (A) and $Ce_{0.5}Fe_{0.5}W_{0.3}O_x$-S (B) catalysts.

SEM and HR-TEM characterization were employed to investigate the effects of tungsten doping on the surface morphology and microstructure of the $Ce_{0.5}Fe_{0.5}O_x$-S catalyst. The results are presented in Figures 5 and 6, respectively. As shown in Fig. 5, all catalysts comprise assemblies of non-uniform stacked nanoparticles, and the doping of tungsten at the molar ratios of 0.1 and 0.3 effectively prevented nanoparticle coalescence, resulting in a more refined and

dispersed morphology [30]. Meanwhile, the enhancement of tungsten doping molar ratio to 0.5 promotes the agglomeration of nanoparticles due to the deposition of WO_3 crystals [31]. From the HR-TEM images in Fig. 6, it can be found that the crystal fringe spacing on the surface of $Ce_{0.5}Fe_{0.5}O_x$-S catalyst is 0.314 nm and 0.277 nm, which belong to the (111) and (200) crystal planes of cubic fluorite structure CeO_2, respectively. Meanwhile, the lattice fringe spacing contracted to 0.307 nm and 0.270 nm in the $Ce_{0.5}Fe_{0.5}W_{0.3}O_x$-S catalyst, confirming the incorporation of W species into the CeO_2 lattice and the resulting lattice distortion [4]. Moreover, no lattice fringes corresponding to WO_3 crystals were observed, indicating that the tungsten oxides are present in an amorphous form in the $Ce_{0.5}Fe_{0.5}W_{0.3}O_x$-S catalyst, consistent with the XRD results shown in Fig. 2.

3.4 XPS and TG-DTG

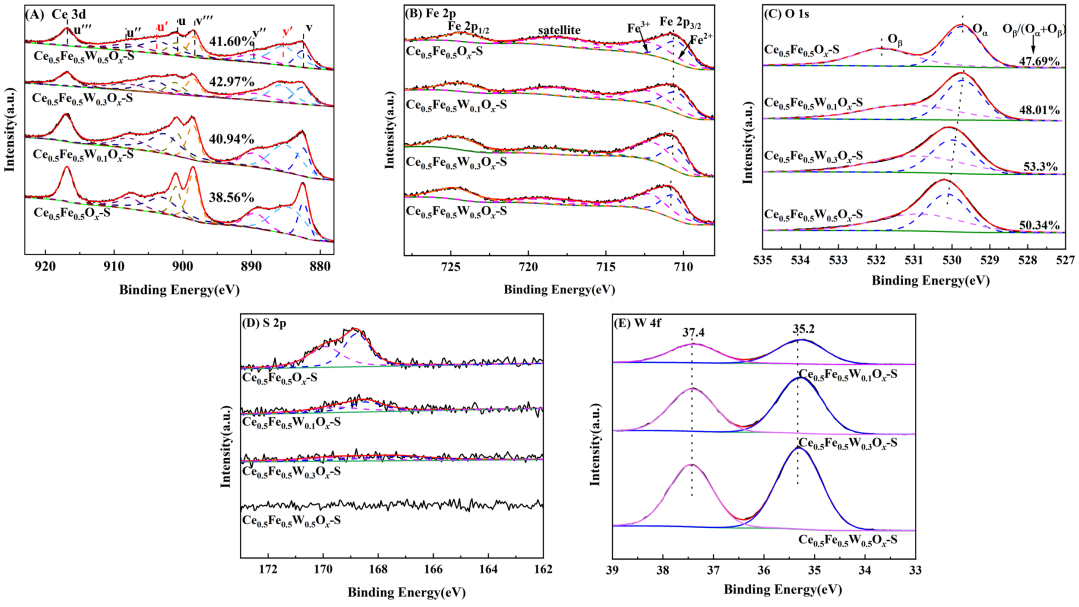

Fig. 7. Influence of tungsten doping on XPS spectra of $Ce_{0.5}Fe_{0.5}O_x$-S catalyst: (A) Ce 3d, (B) Fe 2p, (C) O 1s, (D) S 2p and (E) W 4f.

The effect of tungsten doping on the surface elemental concentrations and relative ratios of the $Ce_{0.5}Fe_{0.5}O_x$-S catalyst was investigated using X-ray photoelectron spectroscopy (XPS), with the results presented in Fig. 7 and Table 2. The deconvoluted Ce 3d spectra in Fig. 7 (A) confirm the co-presence of Ce^{4+} and Ce^{3+} oxidation states in all catalysts, and the formed electron pair of Ce^{3+}/Ce^{4+} is usually thought to promote oxygen vacancies via their electron switching [32,33]. The doping of tungsten increases the surface $Ce^{3+}/(Ce^{3+}+Ce^{4+})$ molar ratio of $Ce_{0.5}Fe_{0.5}O_x$-S catalyst, and $Ce_{0.5}Fe_{0.5}W_{0.3}O_x$-S presents the highest surface $Ce^{3+}/(Ce^{3+}+Ce^{4+})$ molar ratio (42.97%),

indicating that tungsten doping contributes to regulating the interaction of cerium and iron species in $Ce_{0.5}Fe_{0.5}O_x$-S [17]. The Fe 2p spectra in Fig. 7(B) indicate the presence of both Fe^{3+} and Fe^{2+} species in the as-synthesized catalysts. Tungsten doping increases the surface $Fe^{3+}/(Fe^{3+}+Fe^{2+})$ molar ratio of the $Ce_{0.5}Fe_{0.5}O_x$-S catalyst, particularly at a W/(Ce + Fe) doping molar ratio of 0.3. This is consistent with the typical redox reaction $Ce^{4+}+ Fe^{2+} \rightleftharpoons Ce^{3+}+ Fe^{3+}$ observed in cerium-iron mixed oxide catalysts. Therefore, it can be deduced that tungsten doping promotes the above reaction and increases the surface concentrations of both Ce^{3+} and Fe^{3+} [5], although it decreases the concentration of Ce species on the surface of $Ce_{0.5}Fe_{0.5}O_x$-S catalyst effectively. However, tungsten doping has almost no effect on the concentration of iron atoms on the catalyst surface, and the concentration of surface iron species in $Ce_{0.5}Fe_{0.5}W_{0.3}O_x$-S is even higher than that in $Ce_{0.5}Fe_{0.5}O_x$-S, demonstrating there exist promoted electron interaction between iron and tungsten. While, this has also been confirmed by the slight shift in the binding energy of the iron 2p spectrum [34]. The O 1s spectra in Fig. 7 (C) were fitted with two components: lattice oxygen (O_β, 529.8 eV) and chemisorbed oxygen (O_α, 532.8 eV) [35] and tungsten doping increases the surface O_{total} concentration and $O_\alpha/(O_\alpha+O_\beta)$ molar ratio of $Ce_{0.5}Fe_{0.5}O_x$-S catalyst, demonstrating that the promoted interaction of Fe and W contributes to increasing the amount of chemisorbed oxygen, which is generally thought to present stronger mobility than chemisorbed oxygen and plays a key role in the oxidation reaction [36]. Furthermore, the binding energy associated with chemisorbed oxygen (O_α) gradually increases with the rising tungsten doping molar ratio. Notably, $Ce_{0.5}Fe_{0.5}W_{0.3}O_x$-S exhibits the highest surface molar ratio of $O_\alpha/(O_\alpha + O_\beta)$, which may contribute significantly to its outstanding low-temperature NH_3-SCR activity. According to the fitted W $4f_{7/2}$ (35.2 eV) and W $4f_{5/2}$ (37.4 eV) peaks shown in Fig. 7(D), tungsten on the catalyst surface exists predominantly as W^{6+} [37]. Moreover, increasing the tungsten doping molar ratio enhances the intensity of both W $4f_{7/2}$ and W $4f_{5/2}$ peaks, indicating a higher concentration of W^{6+} species in the catalyst.

It should be noted that, as shown in Fig. 7(E) and Table 2, gas-phase sulfation of $COS+CS_2$ facilitates the formation of S^{6+} species, which is recognized to enhance the acid sites and consequently promote the NH_3-SCR catalytic activity [15]. However, tungsten doping decreases the formed amount of S^{6+} on the surface of $Ce_{0.5}Fe_{0.5}O_x$-S catalyst, and this effect is gradually increased with the enhancement of tungsten doping molar ratio from 0.1 to 0.5. Interestingly, no

XPS spectrum of S 2p was detected on the surface of $Ce_{0.5}Fe_{0.5}W_{0.5}O_x$-S catalyst, indicating that the doping of tungsten with W/(Ce+Fe) being 0.5 completely restrains the sulfation of Fe/Ce species and the formation of sulfate on the surface of $Ce_{0.5}Fe_{0.5}O_x$-S catalyst. This indicates that tungsten doping restrains the gas-phase sulfation of Ce/Fe species and reduces the formed amount of sulfates in catalyst, especially the latter, which may be due to the promoted interaction of Fe and W. In order to further determine the effect of tungsten doping on the formation of sulfates on the catalyst surface, the TG-DTG characterization was conducted on the $Ce_{0.5}Fe_{0.5}O_x$-S and $Ce_{0.5}Fe_{0.5}W_{0.3}O_x$-S catalysts, and the results are shown in Fig. 8. It can be found that two catalysts exhibit similar desorption amount of physically adsorbed water or/and hydroxyl at the first stage (< 200 ºC), but $Ce_{0.5}Fe_{0.5}W_{0.3}O_x$-S present less desorption amounts of both weakly adsorbed sulfur at the stage of 200 ºC < T < 600 ºC and metal sulfate decomposition at temperatures higher than 600 ºC [13]. And the content of metal sulfate in $Ce_{0.5}Fe_{0.5}O_x$-S catalyst is reduced by about 76.9 %, which is consistent with the results of XRD and XPS analysis. Therefore, tungsten doping inhibits the adsorption, hydrolysis and oxidation of COS+CS_2 on the surface of $Ce_{0.5}Fe_{0.5}O_x$ catalyst, thereby suppressing the formation of metal sulfates. This also plays a key role in regulating the catalyst's redox properties and surface acid sites.

Table 2. The surface composition and atomic ratio of these catalysts calculated from XPS.

Samples	Atomic concentrations (%)					Atomic ratios (%)		
	Ce	Fe	W	O	S	Ce^{3+}/(Ce^{3+}+Ce^{4+})	Fe^{3+}/(Fe^{2+}+Fe^{3+})	O_β/(O_α+O_β)
$Ce_{0.5}Fe_{0.5}O_x$-S	27.17	6.73	-	63.37	2.73	38.56	73.28	47.69
$Ce_{0.5}Fe_{0.5}W_{0.1}O_x$-S	25.82	6.25	2.93	63.81	1.19	40.94	73.23	48.01
$Ce_{0.5}Fe_{0.5}W_{0.3}O_x$-S	19.42	6.80	6.40	67.16	0.22	42.97	76.11	53.3
$Ce_{0.5}Fe_{0.5}W_{0.5}O_x$-S	16.75	6.66	9.12	67.47	-	41.6	73.95	50.34

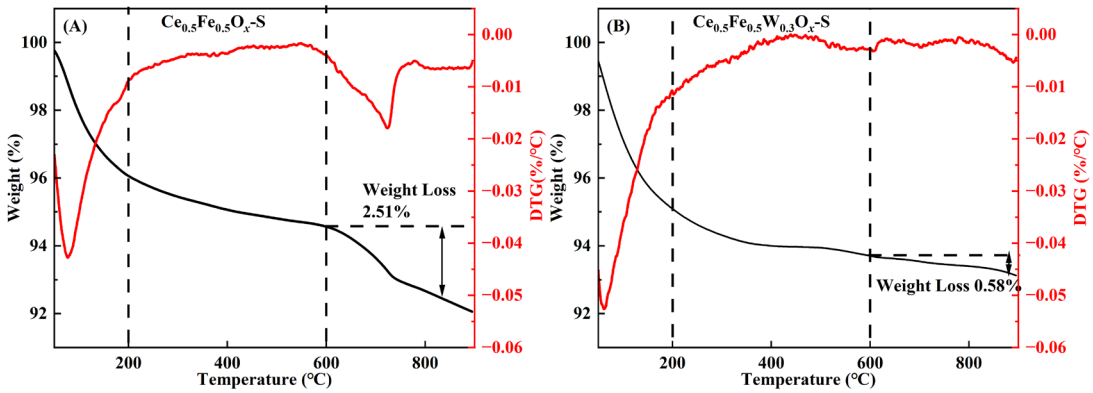

Fig. 8. TG-DTG curves of $Ce_{0.5}Fe_{0.5}O_x$-S and $Ce_{0.5}Fe_{0.5}W_{0.3}O_x$-S catalysts.

3.5 H_2-TPR and NH_3-TPD

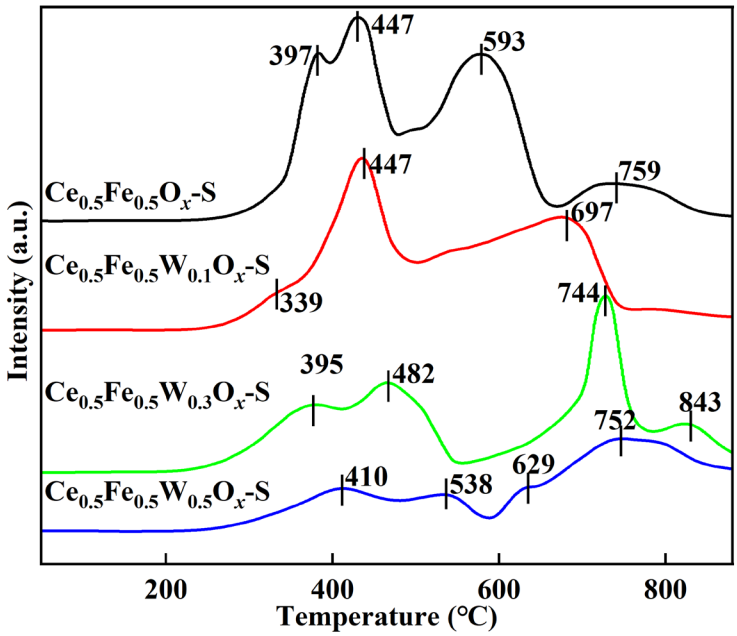

Fig. 9. H_2-TPR profiles of $Ce_{0.5}Fe_{0.5}O_x$-S, $Ce_{0.5}Fe_{0.5}W_{0.1}O_x$-S, $Ce_{0.5}Fe_{0.5}W_{0.3}O_x$-S and $Ce_{0.5}Fe_{0.5}W_{0.5}O_x$-S catalysts.

The influence of tungsten doping on the $Ce_{0.5}Fe_{0.5}O_x$-S catalyst reduction behavior was investigated by H_2 temperature-programmed reduction (H_2-TPR), with the results presented in Fig. 9 and Table S2. As shown in Fig. 9, four distinct reduction peaks at 397 °C, 447 °C, 593 °C, and 759 °C were observed for the $Ce_{0.5}Fe_{0.5}O_x$-S catalyst. These correspond respectively to the reduction of Fe_2O_3 to Fe_3O_4, the reduction of Fe_3O_4 to FeO and/or surface Ce^{4+} to Ce^{3+}, the reduction of FeO to Fe and/or metal sulfates, and the reduction of bulk Ce^{4+} to Ce^{3+} [22]. Tungsten doping decreases the initial H_2-reduction temperature of $Ce_{0.5}Fe_{0.5}O_x$-S catalyst, indicating a promoting effect on the formation of chemisorbed oxygen. And only two broad reduction peaks

are detected for $Ce_{0.5}Fe_{0.5}W_{0.1}O_x$-S catalyst, demonstrating the regulation of tungsten doping on the interaction of cerium and iron species and thereby regulating the redox performance of catalyst. Furthermore, the enhancement of tungsten doping molar ratio gradually decreases the performance of H_2 reduction lower than 600 °C due to the inhibition by WO_3 crystals, especially the catalyst of $Ce_{0.5}Fe_{0.5}W_{0.5}O_x$-S[15]. Interestingly, an obvious reduction peak was detected at 744 °C for $Ce_{0.5}Fe_{0.5}W_{0.3}O_x$-S catalyst, which may be attributed to the reduction of metal sulfate, indicating that the formed metal sulfate in $Ce_{0.5}Fe_{0.5}W_{0.3}O_x$-S presents better dispersion and stronger thermal stability than that of $Ce_{0.5}Fe_{0.5}O_x$-S catalyst, thereby exhibits a sharp and concentrated reduction peak of metal sulfate. Many studies have pointed out that lower initial reduction temperature was beneficial for improving the redox ability and catalytic activity [5,38]. As shown in Table S2, tungsten doping decreases the reduction onset temperature of $Ce_{0.5}Fe_{0.5}O_x$-S catalysts, and thereby improves its redox ability. The initial reduction temperatures of these catalysts decrease as following: $Ce_{0.5}Fe_{0.5}W_{0.3}O_x$-S (241 °C) < $Ce_{0.5}Fe_{0.5}W_{0.5}O_x$-S (243 °C) < $Ce_{0.5}Fe_{0.5}W_{0.1}O_x$-S (250 °C) <$Ce_{0.5}Fe_{0.5}O_x$-S (282 °C), which correlates well with their observed low-temperature catalytic performance. Furthermore, $Ce_{0.5}Fe_{0.5}W_{0.3}O_x$-S exhibits the largest H_2-TPR peak area below 350 °C, indicating its superior low-temperature redox capability [39].

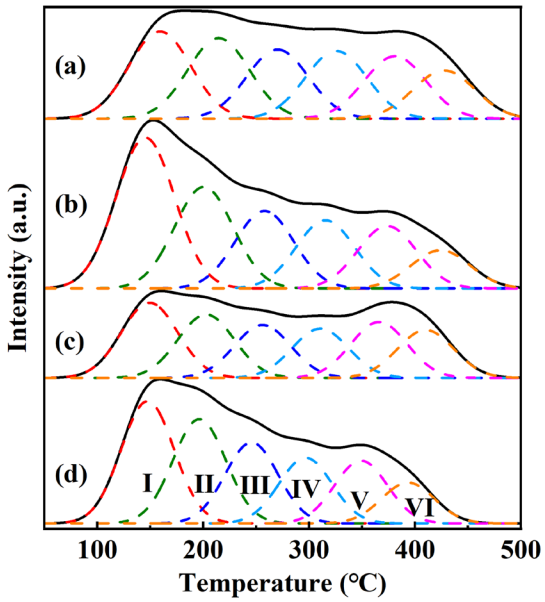

Fig. 10. The NH_3-TPD curves of (a) $Ce_{0.5}Fe_{0.5}O_x$-S, (b) $Ce_{0.5}Fe_{0.5}W_{0.1}O_x$-S, (c) $Ce_{0.5}Fe_{0.5}W_{0.3}O_x$-S and (d) $Ce_{0.5}Fe_{0.5}W_{0.5}O_x$-S catalysts.

Thanks to the excellent solid acid properties of tungsten species, it is widely used as an acid site regulator and anti-SO_2 poisoning additive for catalysts in the NH_3-SCR field. However, according to the above characterization results, tungsten doping reduces the formation amount of metal sulfate in $Ce_{0.5}Fe_{0.5}O_x$ and even completely inhibits its residue in catalyst. Therefore, tungsten doping contributes to regulating the surface acid sites of $Ce_{0.5}Fe_{0.5}O_x$-S catalyst, which were tested by NH_3-TPD. As shown in Fig. 10, there exists a wide desorption peak of NH_3 in the temperature range of 50-500 °C for NH_3-TPD curves, indicating both weak acid sites (below 200 °C) and medium-strong acid sites (200-500 °C) present in the as-synthesized catalysts [40,41]. Furthermore, tungsten doping makes the desorption temperature of NH_3 species shift to low temperature, indicating the promoted effect of tungsten doping on the acid sites of $Ce_{0.5}Fe_{0.5}O_x$-S catalyst. And this promotional effect is further enhanced with the doping molar ratio of W/(Ce+Fe) from 0.1 to 0.5. This demonstrates that tungsten doping contributes to enriching the weak acid sites of $Ce_{0.5}Fe_{0.5}O_x$-S catalyst. However, as shown in Table S3, $Ce_{0.5}Fe_{0.5}W_{0.1}O_x$-S presents larger both total acid sites and weak acid sites/total acid sites proportion than $Ce_{0.5}Fe_{0.5}O_x$-S catalyst. Meanwhile, $Ce_{0.5}Fe_{0.5}W_{0.3}O_x$-S shows the least total acid sites and weak acid sites/total acid sites proportion. Interestingly, increasing the tungsten doping molar ratio from 0.3 to 0.5 results in a further increase in both the total acid sites and the proportion of weak acid sites to total acid sites on the catalyst. Previous studies have indicated that the introduction of sulfate species contributes to the enhancement of acid sites; for example, Cai et al. found when using SO_2 as the sulfur source to conduct gas-phase sulfation of the praseodymium oxides catalyst, an appropriate sulfidation time could effectively control the quantity or type of sulfate deposited on the surface of the praseodymium oxides, thereby significantly enhancing the number and intensity of Brønsted acidic sites of the catalyst [42]. And, the cerium-zirconium solid solution catalyst prepared by Tan et al. after sulfidation showed a change in the acid sites on the catalyst surface, shifting from being dominated by Lewis acid sites to being dominated by Brønsted acid sites. Moreover, the sulfured cerium-zirconium solid solution catalyst exhibited stronger acid site intensity and higher adsorption capacity for NH_3 molecules compared to the un-sulfided [8]. Considering that tungsten doping also reduces the amount of sulfate formed on the catalyst surface, it can be inferred that tungsten oxide solid acids and S^{6+} species play distinct roles in acid site formation in the W-doped $Ce_{0.5}Fe_{0.5}O_x$-S catalyst. Both high sulfate ion content and tungsten doping can independently

increase the total acid sites of the catalyst. Furthermore, numerous studies have confirmed that an optimal balance between redox properties and surface acidity facilitates the adsorption and activation of NH_3 on the catalyst surface [43,44]. Therefore, $Ce_{0.5}Fe_{0.5}W_{0.3}O_x$-S exhibits the highest surface oxygen vacancy concentration and the best NH_3-SCR activity, despite of having the lowest total acid sites and the smallest proportion of weak acid sites to total acid sites.

4. Conclusions

In this study, tungsten doping was employed to regulate the gas-phase sulfation of active components in the $Ce_{0.5}Fe_{0.5}O_x$-S catalyst by organic COS and CS_2. We found that tungsten doping significantly enhanced the low-to-medium temperature NH_3-SCR activity, with an optimal W/(Ce+Fe) molar ratio of 0.3. Characterization results showed that gas-phase COS+CS_2 sulfated the active components of $Ce_{0.5}Fe_{0.5}O_x$-S, particularly the iron species. However, tungsten doping inhibited the adsorption and conversion of COS and CS_2 through a strengthened interaction between iron and tungsten species. This interaction reduced the intensities of α-Fe_2O_3 and cubic fluorite CeO_2 diffraction peaks and caused the disappearance of iron sulfate and α-Fe_2O_3 peaks, with this effect becoming more pronounced as the W/(Ce+Fe) ratio increased from 0.1 to 0.5. Furthermore, this promoted interaction also improved oxygen vacancies of $Ce_{0.5}Fe_{0.5}O_x$-S catalyst and enriched its pore structure, but the formation of WO_3 crystal under the W/(Ce+Fe) molar ratio of 0.5 shielded the Raman peaks of cubic fluorite structure CeO_2 or/and oxygen vacancies on the surface of catalyst, which blocked the partial pore structure and decreased the BET surface area of $Ce_{0.5}Fe_{0.5}O_x$-S catalyst on the contrary. Interestingly, tungsten doping promotes higher surface concentrations of Ce^{3+} and Fe^{3+} species, with $Ce_{0.5}Fe_{0.5}W_{0.3}O_x$-S showing even greater surface Fe content than the undoped catalyst, despite of an overall decrease in Ce species. Additionally, the Fe-W interaction suppresses gas-phase sulfation of Ce and Fe species by COS and CS_2, reducing sulfate formation and thereby modulating the total acid sites and the ratio of weak acid sites to total acid sites. These findings suggest that tungsten oxide solid acid sites and S^{6+} species play distinct roles in acid site formation in W-doped $Ce_{0.5}Fe_{0.5}O_x$-S catalysts. Notably, $Ce_{0.5}Fe_{0.5}W_{0.3}O_x$-S exhibits the highest surface oxygen vacancy concentration and superior NH_3-SCR activity, although it possesses the lowest total acid sites and weak acid site proportion.

The gas-phase sulfation of COS or/and CS_2 treated $Ce_{0.5}Fe_{0.5}W_{0.3}O_x$-S catalyst exhibits excellent

de-nitration efficiency in the medium and low-temperature range, demonstrating its potential for practical industrial applications. Meanwhile, the regulatory effect of tungsten doping on the sulfidation degree of the catalyst provides a theoretical basis for its further optimization and modification. Future research can evaluate the long-term stability and durability of this catalyst in environments containing complex flue gas components (such as SO_2, H_2O, and alkali metals), and explore its scalability and feasibility in industrial-scale tests.

Nomenclature table

Abbreviation	Full Name
2LO	Second-order longitudinal optical mode
BET	Brunauer-Emmett-Teller
COS	Carbonyl sulfide
CS_2	Carbon disulfide
D mode	Defect-induced mode
DTG	Derivative thermogravimetry
F_{2g}	F_{2g} vibrational mode
FTIR	Fourier transform infrared spectroscopy
GHSV	Gas hourly space velocity
H_2-TPR	Temperature programmed reduction of H_2
HR-TEM	High-resolution transmission electron microscopy
HTPB	Hydroxyl-terminated polybutadiene
HTD	High-temperature thermal decomposition
IUPAC	International Union of Pure and Applied Chemistry
NH_3-SCR	Ammonia selective catalytic reduction
NH_3-TPD	Temperature programmed desorption of NH_3
O_α	Chemisorbed oxygen
O_β	Lattice oxygen
PDF	Powder Diffraction File
ppm	Parts per million
Raman	Raman spectroscopy

SEM	Scanning electron microscopy
SI	Supporting Information
TG	Thermogravimetric analysis
TG-DTG	Thermogravimetric-derivative thermogravimetric analysis
vol. %	Volume percent
XPS	X-ray photoelectron spectroscopy
XRD	X-ray diffraction

CRediT authorship contribution statement

Zhibo Xiong: Conceptualization, Funding acquisition, Writing-review & editing. **Jingsong Zhou:** Writing-review & editing, Methodology, Validation. **Mengyao Wang:** Validation and Methodology. **Yafei Zhu:** Validation, Methodology, Writing - original draft. **Zhou Liu:** Validation and Methodology. **Fei Zhou:** Validation and Methodology. **Zhenchang Sun:** Validation and Methodology. **Yanping Du:** Validation and Methodology. **Wei Lu:** Investigation, Supervision and editing, Methodology.

Declaration of Competing Interest

The authors declare that they have no known competing financial interests or personal relationships that could have appeared to influence the work reported in this paper.

Ethics approval and consent to participate

Not applicable. This article does not contain any studies with human participants or animals performed by any of the authors.

Consent for publication

Not applicable. This manuscript does not contain any individual person's data in any form.

Funding

This work was supported by General program of Shanghai Natural Science Foundation (No. 21ZR1461900) and the National Science Foundation of China (No. 51406118).

Availability of data and materials

The datasets generated during and/or analysed during the current study are available from the corresponding

author on reasonable request.

Acknowledgements

Not applicable.

References

[1] Liu J, Ye D, Feng J, Wu S, Zhu K, Guo R (2026) Mechanistic investigation of the promotional effect of $Fe_2(SO_4)_3$ on the SCR performance of CrO_x catalysts. Fuel 415:138504. https://doi.org/10.1016/j.fuel.2026.138504.

[2] Zhang J, Chen LQ, Fan YX, Zhao C, Dai WL, Yang LX, Zhou L, Zou JP, Luo XB (2023) Unraveling the high catalytic activity of single atom Mo-doped TiO_2 toward NH_3-SCR: Synergetic roles of Mo as acid sites and oxygen vacancies as oxidation sites. Chem Eng J 465: 142759. https://doi.org/10.1016/j.cej.2023.142759.

[3] Dong Y, Zhang D, Xu Y, Ye D, Guo R (2026) Getting insights into the synergistic effects of Zn and HCl on the SCR performance of the CeO_2-TiO_2 catalyst. Energy Fuels 40:1360–1367. https://doi.org/10.1021/acs.energyfuels.5c05850.

[4] Li MF, Gao M, He GZ, Yu YB, He H (2023) Mechanistic Insight into the Promotion of the Low-Temperature NH_3-Selective Catalytic Reduction Activity over $Mn_xCe_{1-x}O_y$ Catalysts: A Combined Experimental and Density Functional Theory Study. Environ. Sci. Technol. 57: 3875-3882. https://doi.org/10.1021/acs.est.2c08608.

[5] Tang XL, Shi YR, Gao FY, Zhao SZ, Yi HH, Xie ZL (2020) Promotional role of Mo on $Ce_{0.3}FeO_x$ catalyst towards enhanced NH_3-SCR catalytic performance and SO_2 resistance. Chem Eng J 398: 125619. https://doi.org/10.1016/j.cej.2020.125619.

[6] Zhou ZZ, Li WH, Liu ZM (2021) Significantly Enhanced Catalytic Performance of $Fe_2(SO_4)_3/CeO_2$ Catalyst for the Selective Catalytic Reduction of NO_x by NH_3. Ind Eng Chem Res 60: 15472-15478. https://doi.org/10.1021/acs.iecr.1c02977.

[7] Ye D, Feng JY, Xu YF, You YH, Gao SJ, Guo RT, Zhu K (2024) New insights into the various SCR performance of the CeO_x-FeO_x mixed-oxide catalysts prepared using different iron precursors. J Energy Inst 114: 101593. https://doi.org/10.1016/j.joei.2024.101593.

[8] Tan W, Wang JM, Li LL, Liu AN, Song G, Guo K, Luo YD, Liu FD, Gao F, Dong L (2020) Gas phase sulfation of ceria-zirconia solid solutions for generating highly efficient and SO_2 resistant NH_3-SCR catalysts for NO removal. J Hazard Mater 388: 121729. https://doi.org/10.1016/j.jhazmat.2019.121729.

[9] Wang XB, Guo N, Peng JQ, Wang Y, Li HJ, Ren DD, Gui KT (2023) Excellent operating temperature window and H_2O/SO_2 resistances of Fe-Ce catalyst modified by different sulfation strategies for NH_3-SCR reaction. Environ Sci Pollut Res 30: 50635-50648. https://doi.org/10.1007/s11356-023-25912-x.

[10] Kang KK, Zhao WX, Rong J, Luo W, Long LL, Chen Y, Yao XJ (2022) Effect of H_2SO_4 pretreatment on alkali-resistance performance of $FeZrCeTiO_x$/TNT catalyst for NH_3-SCR reaction. Appl Surf Sci 598: 153774. https://doi.org/10.1016/j.apsusc.2022.153774.

[11] Song ZX, Mo DJ, Zhang XJ, Mao YL, Liu XP, Zhang JH, Liu W, Chen X, Huang ZZ (2024) Mechanism of gas-phase sulfur modified Fe-Ce catalysts in the NH_3-SCR reaction. Mol Catal 569: 2468-8231. https://doi.org/10.1016/j.mcat.2024.114635.

[12] Wang W, Xiong ZB, Jin J, Lu W, Shi HC (2021) Influence of CS_2 pretreatment on the NH_3-SCR activity of CeO_2: Synergistic promotional effect of sulfation and reduction. J Environ Chem Eng 9 :106836. https://doi.org/10.1016/j.jece.2021.106836.

[13] Xiong ZB, Sun ZC, Liu JX, Du YP, Zhu YF, Zhou F, Jin J, Yang QG, Lu W (2024) Influence of organic sulfur gas-phase sulfation on the NH_3-SCR activity of CeO_2 catalyst: The competitive adsorption and conversion of CS_2 and COS at a low hydrolysis temperature. Fuel 364: 131101. https://doi.org/10.1016/j.fuel.2024.131101.

[14] Liu JX, Zhu YF, Sun ZC, Du YP, Xiong ZB, Zhou F, Jin J, Yang QG, Lu W (2023) Promotional effect of H_2O introduction on the NH_3-SCR activity of the gas-phase sulfated CeO_2 catalyst by organic CS_2+COS: Influence of H_2O concentration. J Environ Chem Eng 11: 111529. https://doi.org/10.1016/j.jece.2023.111529.

[15] Xiong ZB, Zhu YF, Liu JX, Du YP, Zhou F, Jin J, Yang QG, Lu W (2024) The influence of H_2O or/and O_2 introduction during the low-temperature gas-phase sulfation of organic COS+CS_2 on the conversion and deposition of sulfur-containing species in the sulfated CeO_2-OS catalyst for NH_3-SCR. Nanoscale 16: 1223. https://doi.org/10.1039/d3nr04686a.

[16] Wang XR, Yang CQ, Wu DP, Han Q, Jin SL, Zhang R, Jin ML, Wang ZY, Wang JT, Ling LC (2025) The enhanced SO_2 resistance of Fe-Ti catalyst by W/SO_4^{2-} co-modification for NH_3-SCR: A combined experimental and DFT study. Sep Purif Technol 357: 130167. https://doi.org/10.1016/j.seppur.2024.130167.

[17] Cheng K, Tang S, Feng JL, An MZ, Zhu JJ, Xia MG (2024) Broadening active temperature window for NH_3-SCR on tungsten-promoted $MnCeO_x$ nanorod catalysts. Process Saf Environ Prot 182: 1-10. https://doi.org/10.1016/j.psep.2023.11.070.

[18] Nam KB, Kwon DW, SunHong SC (2017) DRIFT study on promotion effects of tungsten-modified Mn/Ce/Ti

catalysts for the SCR reaction at low-temperature. Appl Catal A Gen 542: 55-62. http://dx.doi.org/10.1016/j.apcata.2017.05.017.

[19] Arfaoui J, Ghorbel A, Petitto C, Delahay G (2018) Novel V_2O_5-CeO_2-TiO_2-SO_4^{2-} nanostructured aerogel catalyst for the low temperature selective catalytic reduction of NO by NH_3 in excess O_2. Appl Catal B Environ 224: 264-275. https://doi.org/10.1016/j.apcatb.2017.10.059.

[20] Li XD, Han ZT, Wang XX, Yang SL, Liu G, Gao Y, Li CL (2022) Acid treatment of ZrO_2-supported CeO_2 catalysts for NH_3-SCR of NO: Influence on surface acidity and reaction mechanism. J Taiwan Inst Chem Eng 132: 104144. https://doi.org/10.1016/j.jtice.2021.11.011.

[21] Zhang YK, Xiong ZB, Yang QG, Zhou F, Lu W, Shi HC (2022) Influence of copper doping on the low-medium NH_3-SCR activity of magnetic W/Fe_2O_3 catalyst: Its synergetic effect of glucose dosage. J Environ Chem Eng 10: 108694. https://doi.org/10.1016/j.jece.2022.108694.

[22] Si ZP, Shen YJ, He JB, Yan TT, Zhang JP, Deng J, Zhang DS (2022) SO_2-Induced Alkali Resistance of $FeVO_4$/TiO_2 Catalysts for NO_x Reduction. Environ Sci Technol 56: 605-613. https://doi.org/10.1021/acs.est.1c05686.

[23] Zhang XJ, Wang JK, Song ZX, Zhao H, Xing Y, Zhao M, Zhao JG, Ma Z, Zhang PP, Tsubaki N (2019) Promotion of surface acidity and surface species of doped Fe and SO_4^{2-} over CeO_2 catalytic for NH_3-SCR reaction. Mol Catal 463: 1-7. https://doi.org/10.1016/j.mcat.2018.11.002.

[24] Mu JC, Li XY, Sun WB, Fan SY, Wang XY, Wang L, Qin MC, Gan GQ, Yin ZF, Zhang DK (2018) Inductive Effect Boosting Catalytic performance of Advanced $Fe_{1-x}V_xO_\delta$ Catalysts in Low-Temperature NH_3 Selective Catalytic Reduction: Insight into the Structure, Interaction, and Mechanisms. ACS Catal 8: 6760-6774. https://doi.org/10.1021/acscatal.8b01196.

[25] Liu XS, Jiang P, Chen Y, Wang YG, Ding QL, Sui ZM, Chen HF, Shen ZY, Wu XD (2021) A basic comprehensive study on synergetic effects among the metal oxides in CeO_2-WO_3/TiO_2 NH_3-SCR catalyst. Chem Eng J 421: 127833. https://doi.org/10.1016/j.cej.2020.127833.

[26] Xiong ZB, Liu JX, LiJ, Du YP, Zhou F, Yang QG, Wang W, Lu W, Shi HC (2023) Insight into the regulating effect of phosphorylation on the NH_3-SCR activity and properties of thiourea modified CeO_2-TA catalyst. Mol Catal 548: 113454. https://doi.org/10.1016/j.mcat.2023.113454.

[27] Iwasaki M, Dohmae K, Nagai Y, Sudo E, Tanaka T (2028) Experimental assessment of the bifunctional NH_3-SCR pathway and the structural and acid-base properties of WO_3 dispersed on CeO_2 catalysts. J Catal 359: 55-67. https://doi.org/10.1016/j.jcat.2017.12.032.

[28] Chen SJ, Xie RY, Liu ZS, Ma L, Yan NQ (2023) Efficient NO_x Reduction against Alkali Poisoning over a Self-Protection Armor by Fabricating Surface $Ce_2(SO_4)_3$ Species: Comparison to Commercial Vanadia Catalysts. Environ Sci Technol 57: 2949-2957. https://doi.org/10.1021/acs.est.2c08570.

[29] Xiong YR, Wang LL, Ning P, Luo JF, Li X, Yuan L, Xie YB, Ma YX, Wang XQ (2024) Constructing oxygen vacancy-enriched Fe_3O_4@MnO_2 core-shell nanoplates for highly efficient catalytic oxidation of H_2S in blast furnace gas. Sep Purif Technol 336: 126234. https://doi.org/10.1016/j.seppur.2023.126234.

[30] Ke SR, Min X, Liu YG, Mi RY, Wu XW, Huang ZH, Fang MH. (2022) Tungsten-Based Nanocatalysts: Research Progress and Future Prospects. Molecules 27: 4751. https://doi.org/10.3390/molecules27154751

[31] Wang CZ, Yang SJ, Chang HZ, Peng Y, Li JH. (2013) Dispersion of tungsten oxide on SCR performance of $V_2O_5WO_3/TiO_2$: Acidity, surface species and catalytic activity. Chem. Eng. J. 225:520–527.https://doi.org/10.1016/j.cej.2013.04.005

[32] Zhou ZZ, Lan JM, Liu LY, Liu ZM (2021) Enhanced alkali resistance of sulfated CeO_2 catalyst for the reduction of NO_x from biomass fired flue gas. Catal Commun 149: 106230. https://doi.org/10.1016/j.catcom.2020.106230.

[33] Zhang H, Lian ZH, Lin CX, Zhu Y, Shan WP, He H (2023) Insight into the mechanisms of activity promotion and SO_2 resistance over Fe-doped Ce-W oxide catalyst for NO_x reduction. J Colloid Interface Sci 652: 923-935. https://doi.org/10.1016/j.jcis.2023.08.129.

[34] Zhang QL, Zhang YQ, Zhang TX, Wang HM, Ma YP, Wang JF, Ning P (2020) Influence of preparation methods on iron-tungsten composite catalyst for NH_3-SCR of NO: The active sites and reaction mechanism. Appl Surf Sci 503: 144190. https://doi.org/10.1016/j.apsusc.2019.144190.

[35] Zhao WX, Rong J, Luo W, Long LL, Yao XJ (2022) Enhancing the K-poisoning resistance of CeO_2-SnO_2 catalyst by hydrothermal method for NH_3-SCR reaction. Appl Surf Sci 579: 152176. https://doi.org/10.1016/j.apsusc.2021.152176.

[36] Guo DY, Guo RT, Duan CP, Liu YZ, Wu GL, Qin Y, Pan WG (2021) The enhanced K resistance of Cu-SSZ-13 catalyst for NH_3-SCR reaction by modification with Ce. Mol Catal 502: 111392. https://doi.org/10.1016/j.mcat.2021.111392.

[37] Xiong ZB, Ning X, Zhou F, Yang B, Tu YW, Jin J, Lu W, Liu ZH (2018) Environment-friendly magnetic Fe–Ce–W catalyst for the selective catalytic reduction of NO_x with NH_3: Influence of citric acid content on its activity-structure relationship. RSC Adv 8: 21915. https://doi.org/10.1039/c8ra03131b.

[38] Zhang H, Zou Y G, Peng Y (2017) Influence of sulfation on CeO_2-ZrO_2 catalysts for NO reduction with NH_3. Chin J Catal 38: 160-167. https://doi.org/10.1016/S1872-2067(16)62581-0.

[39] Li J, Zhou F, Xiong ZB, Du YP, Yang QG, Wang W, Lu W (2023) Promotional Effect of Zirconium Doping on the NH_3-SCR Activity of CeO_2 and CeO_2-TA Modified by Thiourea: A Comparative Study. ChemCatChem 15: e202201578. https://doi.org/10.1002/cctc.202201578.

[40] Li W, Zhang C, Li X, Tan P, Zhou A, Fang QY, Chen G (2018). Ho-modified Mn-Ce/TiO_2 for low-temperature SCR of NO_x with NH_3: Evaluation and characterization. Chin J Catal 39: 1653-1663. https://doi.org/10.1016/S1872-2067(18)63099-2

[41] Xu SY, Yin LT, Wang HM, Gao LY, Tian XY, Chen JJ, Zhang QL, Ning P (2022) Improved alkali-tolerance of FeO_x-WO_3 catalyst for NO removal via in situ reserving FeO_x active species. Sep Purif Technol 300: 121824. https://doi.org/10.1016/j.seppur.2022.121824.

[42] Cai YD, Yang P, Liu QL, Ma KL, Ma WX, Song W, Qian QH, Gao F, Tan W, Dong L (2023) Getting insights into gas-phase sulfation effect on catalytic performance of praseodymium oxides in NH_3-SCR of NO. J Rare Earths 41 (2023) 952-958. https://doi.org/10.1016/j.jre.2022.12.004.

[43] Chen JZ, Guo LY, Zhu HC, Qiu Y, Yin DJ, Zhang T, Chen JJ, Peng Y, Li JH (2021) Balancing redox and acidic properties for optimizing catalytic performance of SCR catalysts: A case study of nanopolyhedron CeO_x-supported WO_x. J Environ Chem Eng 9: 105828. https://doi.org/10.1016/j.jece.2021.105828.

[44] Yang R, Gao ZH, Sun M, Fu GY, Cheng G, Liu WY, Yang XB, Zhao XY, Yu L (2021) A highly active VO_x-MnO_x/CeO_2 for selective catalytic reduction of NO: The balance between redox property and surface acidity. J Rare Earths 39: 1370-1381. https://doi.org/10.1016/j.jre.2020.09.006.